# Anomalous small-angle X-ray scattering study of $Tb_xCu_{1-x}$ and $Gd_xCu_{1-x}$ amorphous alloys



1992 J. Phys.: Condens. Matter 4 9709

(http://iopscience.iop.org/0953-8984/4/48/023)

J. Phys.: Condens. Matter 4 (1992) 9709–9720. Printed in the UK

# Anomalous small-angle x-ray scattering study of $Tb_xCu_{1-x}$ and $Gd_xCu_{1-x}$ amorphous alloys

M Maret†, J P Simon†, B Boucher‡, R Tourbot‡ and O Lyon§

† Laboratoire de Thermodynamique et Physico-Chimie Métallurgiques, Unité de Recherche associée au CNRS 29, Ecole Nationale Supérieure d'Electrochimie et d'Electrométallurgie de Grenoble, BP 75, 38402 Saint Martin d'Hères Cédex, France

‡ Service de Physique de l'Etat Condensé, Centre d'Etudes de Saclay, 91191 Gif-sur-Yvette Cédex, France

§ Laboratoire d'Utilisation du Rayonnement Electromagnétique, Bâtiment 209 D, 91405 Orsay Cédex, France

Received 28 July 1992

**Abstract.** Anomalous small-angle x-ray scattering measurements were performed on as-sputtered $Tb_xCu_{1-x}$ ($x = 0.25$ and 0.65) amorphous alloys below the Cu K edge and the Tb $L_{III}$ edge, in order to determine the nature of the particles dispersed in the amorphous matrix. For technical reasons, measurements were also carried out on amorphous $Gd_xCu_{1-x}$ ($x = 0.29$ and 0.7) and the isomorphous behaviours of the two alloys were checked. For the samples studied, the changes in the scattering ring intensity measured near both edges are consistent with the existence of rare-earth hydride particles, the associated decrease in the rare-earth concentration in the amorphous matrix being included in the anomalous scattering variations. From one sample to another, the hydride particles have radii of gyration ranging from 5 to 30 Å and occupy volume fractions from 5 to 20%. Their molecular volumes are close to that of the rare-earth trihydride ($V_{REH_3} \simeq 40$ Å$^3$); some porosity in the hydride particles could explain the larger values (about 48 Å$^3$) found in two samples.

## 1. Introduction

The medium-range order in $Tb_xCu_{1-x}$ ($0.22 < x < 0.65$) metallic glasses prepared by sputtering has been extensively investigated at different temperatures ($2.6\,K < T < 300$ K) by means of small-angle neutron scattering (SANS) (Boucher *et al* 1983, 1986, 1988, Boucher and Chieux 1991). The nuclear SANS intensity of such glasses is characterized at low momentum transfer values ($q = (4\pi \sin\theta)/\lambda$) by a strong decrease and at higher $q$ by a well defined ring. For the composition $Tb_{22}Cu_{78}$, the existence of a nuclear scattering ring at $q \approx 0.2$ Å$^{-1}$ was associated preferentially with Tb hydrides (contamination by hydrogen was clearly revealed by large-angle neutron scattering (Chieux *et al* 1984)). For $T < 20$ K a magnetic ring also observed at 0.2 Å$^{-1}$ showed large magnetization per unit volume and was attributed to asperromagnetic Tb rather than to Tb hydrides which by analogy with crystalline Tb hydrides would be expected to be sperromagnetic (Boucher *et al* 1986). For $x = 0.33$ and 0.5, such an interpretation would still be valid. For $x = 0.65$, the size of the magnetic bubbles was found to be half that of the nuclear bubbles; this difference was interpreted as due to magnetic moments which are better ordered

0953-8984/92/489709+12$07.50  

at the centre. From magnetic SANS measurements, the asperromagnetic character of the magnetic order in bubbles is well indicated; therefore Tb bubbles seem to be the more probable solution. However, asperromagnetic amorphous Tb hydride as another solution cannot be completely eliminated.

Since the magnetic and nuclear scattering rings stem from the same particles, another technique for determining the nature of these particles is anomalous small-angle x-ray scattering (ASAXS) using synchrotron radiation, which is based on the rapid change in the x-ray scattering factor of one element when approaching one of its absorption edges. Since the SAXS intensity of two-phase systems is proportional to the square of the difference between the mean electronic densities of the two phases, measurements at different energies chosen near one absorption edge of both elements must allow us to identify these particles. This technique was applied successfully to the study of clusters of titanium hydrides in amorphous CuTi (Goudeau *et al* 1987) and recently to segregation in amorphous $(FeMn)_{35}Y_{65}$ (Maret *et al* 1989).

This paper is devoted to the analysis of the scattering ring observed in $Tb_xCu_{1-x}$ metallic glasses using the ASAXS technique. In order to select reliably the most probable solution of the possible heterogeneities, it is necessary to perform ASAXS measurements near the absorption edges of both species: here the $L_{III}$ edge of Tb (7515 eV) and the K edge of Cu (8979 eV). However, quantitative measurements near the Cu K edge were expected to be difficult because of the closeness of the $L_I$ (8716 eV) and $L_{II}$ (8252 eV) edges of Tb, which would give a large level of fluorescence superimposed on the scattering signal. In order to reduce the fluorescence of Tb due to the L edges, we decided to substitute Tb by Gd atoms since the $L_I$ (8376 eV) and $L_{II}$ (7930 eV) edges of Gd are farther from the Cu edge than are the L edges of Tb. The isomorphous behaviours of Tb and Gd atoms were checked. Nevertheless the fluorescence was still too intense in the samples 15 $\mu$m thick, previously used in SANS measurements. ASAXS measurements were finally performed in thinner (4–10 $\mu$m) amorphous films deposited on a mica sheet and compared with the results obtained for thicker samples.

## 2. Experimental technique

### *2.1. Sample preparation*

The samples of $Tb_xCu_{1-x}$ ($x = 0.25$ and 0.65) and $Gd_xCu_{1-x}$ ($x = 0.29$ and 0.7) were prepared by sputtering in an argon plasma. Amorphous films thicker than 15 $\mu$m were deposited directly on an aluminium holder cooled to about 77 K. The films thinner than about 10 $\mu$m were too brittle to be used subsequently in the sample changer of the ASAXS spectrometer; they were then deposited on an intermediate mica sheet from 20 to 40 $\mu$m thick pressed on the aluminium holder. The nominal compositions and thicknesses are given in table 1 for samples S1–S8. It is well known that the sputtering process introduces variations in composition depending on the apparatus quality. Thus, the ratios of rare-earth (RE) to copper in the thin films controlled by microprobe analysis could differ from the nominal compositions of the target by from 1 to 3%; impurities such as argon, oxygen and silicon were also detected. Previous measurements also showed the existence of hydrogen the amount of which depends on the fabrication process and is not perfectly reproducible.

### 2.2. *ASAXS measurements*

The ASAXS experiments were performed on the beam line D22 of the synchrotron radiation facility of the Laboratoire d'Utilisation du Rayonnement Electromagnétique in Orsay using a double $Ge_{111}$ monochromator and a linear position-sensitive detector (Dubuisson *et al* 1986). The anomalous measurements were carried out over the following x-ray energy ranges: [6525, 7224 eV] below the Gd $L_{III}$ edge at 7243 eV, [6811, 7495 eV] below the Tb $L_{III}$ edge at 7515 eV and [8700, 8973 eV] below the Cu K edge at 8979 eV. Two sample-to-detector distances of 296 and 523 mm were used for the thick films and the thin films, respectively, deposited on mica, allowing us to cover the respective [0.05, 0.55 $Å^{-1}$] and [0.015, 0.25 $Å^{-1}$] $q$-ranges. The amorphous films were placed perpendicular to the incident x-ray beam (0.3 mm high and 1–3 mm wide) in the automatic sample changer under vacuum. The transmission measurements were made through two monitor scintillators facing polymer films placed before and after the sample. To reduce the fluorescence-noise-to-elastic-signal ratio, a zinc filter (about 50 $\mu$m thick) was placed after the sample. This Zn filter absorbs twice the amount of L-edge fluorescence as it does elastic scattering and therefore increases the signal-to-noise ratio by a factor of 2.

The scattering intensities were corrected (Lyon and Simon 1987) for background, and eventually for the mica and zinc filters, sample absorption and detector efficiencies in position and in energy and were normalized with respect to Ni fluorescence. Finally, the remaining $q$-independent contributions of fluorescence and Raman scattering were subtracted assuming a Porod asymptotic scattering behaviour in $q^{-4}$ at large momentum transfers.

### 2.3. *Atomic scattering factors*

At small momentum transfers, the x-ray atomic scattering factors depend only on the photon beam energy $E$ and are expressed as

$$f_i(E) = Z_i + f_i'(E) + if_i''(E).$$

For species i, $Z_i$ is the atomic number and $f_i'(E)$ and $f_i''(E)$ are the dispersion terms. The values of $f_i'(E)$ and $f_i''(E)$ used for Cu, Tb and Gd elements are those obtained by Sazaki (1984) corrected for the wide energy band of the $Ge_{111}$ monochromator. For the $L_{III}$ edge, $f_{Tb}'(E)$ varies from $-8$ electrons (6811 eV) to $-16$ electrons (7495 eV) and, for the K edge, $f_{Cu}'(E)$ varies from $-3$ electrons (8700 eV) to $-7$ electrons (8973 eV).

## 3. Results

Figures 1 and 2 illustrate the changes in the intensity $I_{at}(q, E)$ (in electrons squared per atom) of the scattering ring centred around 0.2 $Å^{-1}$ measured for a RE-rich amorphous alloy of $Gd_{70}Cu_{30}$ (18 $\mu$m thick; sample S3) near the Gd and Cu edges, respectively. A decrease in the intensity is recorded when moving near the Gd and Cu edges. Figures 3 and 4 show the changes in the scattering ring centred at 0.07 Å for a RE-poor alloy of $Tb_{25}Cu_{75}$ (11 $\mu$m thick; deposited on mica; sample S6) which are strongly different from those of sample S3, i.e. a small increase in $I_{at}(q, E)$ when moving near the Tb edge and a large decrease near the Cu edge. In comparison with

the data shown in figure 2, the accuracy of those in figure 4 is clearly better; this is due to the position of the ring at smaller $q$ and also to the thinness of the sample. In table 1 are listed the most relevant quantities obtained from the ASAXS measurements such as the maximum $q_m$ of the scattering ring, the measured particle radius $R_g$ of gyration and the integrated intensities $\bar{I}(E)$ averaged over an edge. The values of $R_g$ were deduced from Guinier fits calculated beyond the maximum. The integrated intensities per volume unit are given by

$$\bar{I}(E) = \frac{1}{v_{am}} \int_{0.5q_m}^{q_{max}} I_{at}(q, E) q^2 \, dq. \tag{1}$$

$q_{max}$ is the upper limit of the investigated $q$-range and $v_{am}$ is the mean atomic volume of the amorphous alloy for the nominal composition ($v_{am} = \sum_i x_i v_i^0$, i = RE, Cu and $v_i^0$ are the atomic volumes of pure metals). The $q^{-4}$ Porod asymptotic behaviour is too inaccurate to give a reliable corrected value of $\bar{I}(E)$. Nevertheless, since $q_{max}$ was usually about twice the ring position $2q_m$, the underestimation of $\bar{I}(E)$ is about 10–20%. As will be shown in the next section, the scaling functions of the different samples have roughly the same shape; the choice of an almost fixed $q$-range in relative units $[0.5q_m, \simeq 2q_m]$ therefore allows a comparison of the samples.

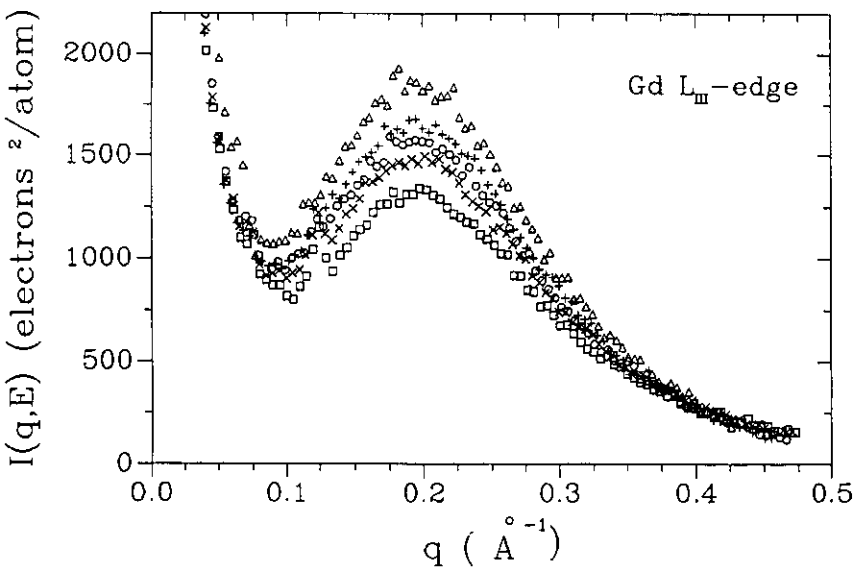


**Figure 1.** Change in the scattering intensity with photon energy near the Gd $L_{III}$ edge for the as-sputtered $Gd_{70}Cu_{30}$ glass (sample S3): Δ, 6525 eV; +, 6965 eV; O, 7129 eV; ×, 7197 eV; □, 7224 eV.

The relative variations $\Delta I/I$ in the scattering ring intensity, given in table 2, are calculated using integral values in order to improve the statistics such as

$$\frac{\Delta I}{I} = \left( \int_{0.5q_m}^{1.5q_m} I_{at}(q, E_{max}) \, dq - \int_{0.5q_m}^{1.5q_m} I_{at}(q, E_{min}) \, dq \right) \Big/ \int_{0.5q_m}^{1.5q_m} I_{at}(q, E_{min}) \, dq. \tag{2}$$

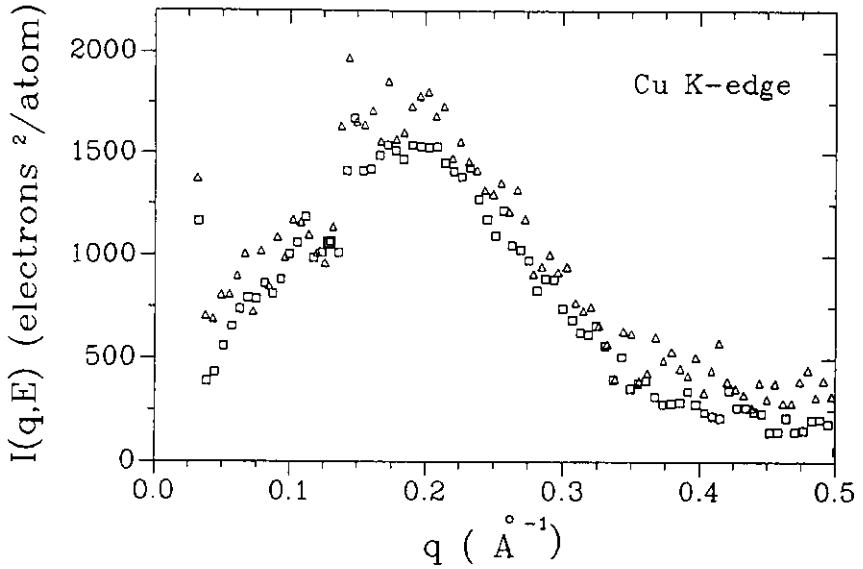


**Figure 2.** Change in the scattering intensity with photon energy near the Cu K edge for the as-sputtered $Gd_{70}Cu_{30}$ glass (sample S3): △, 8700 eV; □, 8973 eV.

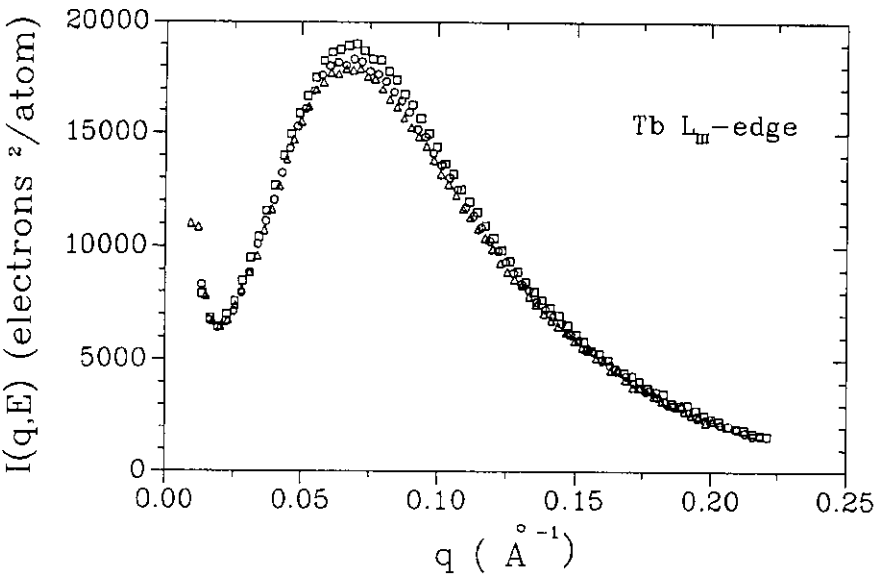


**Figure 3.** Change in the scattering intensity with photon energy near the Tb $L_{III}$ edge for the as-sputtered $Tb_{25}Cu_{75}$ (sample S6): △, 6811 eV; ○, 7402 eV; □, 7495 eV.

$E_{min}$ and $E_{max}$ are respectively the farthest and the nearest energies from the absorption edge. The $q$-range is chosen as the most significant.

From table 1, it is worth emphasizing that, for all the amorphous films deposited directly on the aluminium holder, the scattering ring is centred at around 0.2 $Å^{-1}$ and associated with particles of the same size (about 5 Å); it confirms that the $Tb_xCu_{1-x}$

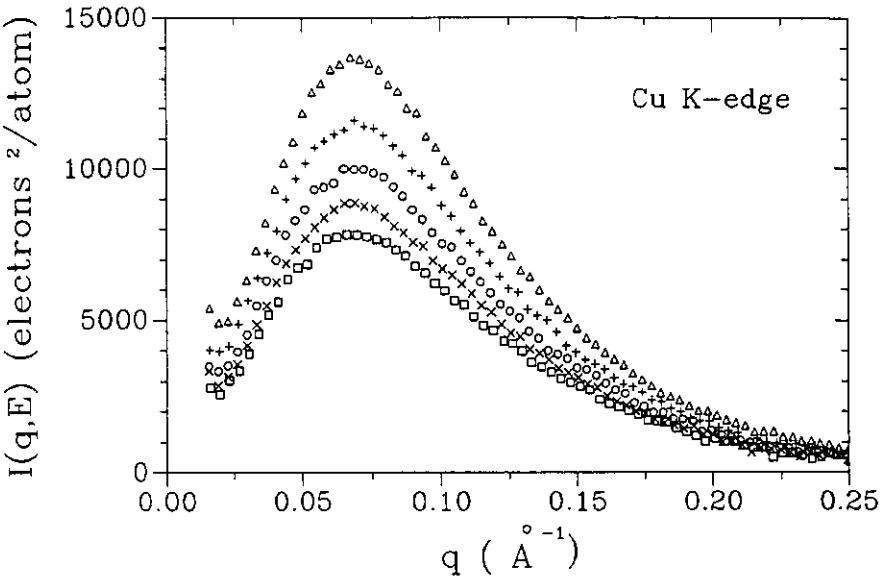


**Figure 4.** Change in the scattering intensity with photon energy near the Cu K edge for the as-sputtered $Tb_{25}Cu_{75}$ (sample S6): △, 8700 eV; +, 8880 eV; ○, 8940 eV; ×, 8966 eV; □, 8973 eV.

and $Gd_xCu_{1-x}$ alloys exhibit similar small-angle scattering. By contrast, the thin films deposited on mica present various positions of the ring from 0.03 to 0.15 $Å^{-1}$ and different sizes of particles; these results suggest that the thin films were not uniformly cooled and that particles were able to grow during the preparation.

For one alloy composition the relative variation in intensity when near an edge varies from one preparation to another and there is no straightforward correlation between $\Delta I/I$ and $q_m$. Nevertheless, for the RE-poor amorphous films, the sign of $\Delta I/I$ for both edges is the same for both $Gd_{29}Cu_{71}$ and $Tb_{25}Cu_{75}$ and their orders of magnitude are rather similar; this again confirms the isomorphism of the two alloys. For the RE-rich alloys, there are some discrepancies which will be analysed in the next section.

## 4. Discussion

### *4.1. Two-phase model*

For a system of volume $V$ containing $N_p$ particles of volume $V_p$ and homogeneous electronic density $\rho_p(E)$ dispersed in a matrix of mean electronic density $\rho_m(E)$, the SAXS intensity per cubic ångström can be expressed as

$$I(q,E) = (N_pV_p^2/V)[\rho_m(E) - \rho_p(E)][\rho_m(E) - \rho_p(E)]^* S(q). \quad (3)$$

$S(q)$ is the Fourier transform of the Patterson function of particles, and the asterisk indicates the complex conjugate. $\rho_i(E) = f_i(E)/v_i$ ($i \equiv$ m, p); $f_m(E)$ and $f_p(E)$ are the mean scattering factors of the surrounding matrix and the particle, respectively. $v_m$ is the mean atomic volume of the matrix and $v_p$ the molecular

**Table 1.** Nominal compositions, thicknesses and atomic volumes of the eight amorphous samples studied; positions $q_m$ of the interference ring and radii $R_g$ of gyration of particles; average integrated intensities of the scattering ring measured near the $L_{III}$ and K edges; molecular volume $v_{hyd}$ and volume fraction $\varphi$ of hydride particles.

| Sample | Alloy | Thickness ($\mu$m) | $v_{am}$ (Å$^3$) | Mica substrate | $q_m$ (Å$^{-1}$) | $R_g$ (Å) | $\bar{I}$ (electrons Å$^{-3}$) RE $L_{III}$ edge | $\bar{I}$ (electrons Å$^{-3}$) Cu K edge | $v_{hyd}$ (Å$^3$) | $\varphi$ |
|---|---|---|---|---|---|---|---|---|---|---|
| S1 | $Gd_{29}Cu_{71}$ | 16 | 18 | No | 0.22 | 5 | 0.77 | Not measured | 40 | 0.12 |
| S2 | $Gd_{29}Cu_{71}$ | 5.5 | 18 | Yes | 0.13 | 12 | 0.4 | 0.27 | 43 | 0.04 |
| S3 | $Gd_{70}Cu_{30}$ | 18 | 26.7 | No | 0.2 | 5 | 0.67 | 0.69 | 48 | 0.12 |
| S4 | $Gd_{70}Cu_{30}$ | 7.5 | 26.7 | Yes | 0.03 | 30 | 0.33 | 0.37 | 41.5 | 0.18 |
| S5 | $Tb_{25}Cu_{75}$ | 15 | 16.8 | No | 0.21 | 5 | 0.99 | Not measured | 38.5 | 0.13 |
| S6 | $Tb_{25}Cu_{75}$ | 11.5 | 16.8 | Yes | 0.07 | 15 | 1.06 | 0.64 | 48 | 0.07 |
| S7 | $Tb_{25}Cu_{75}$ | 7.5 | 16.8 | Yes | 0.15 | 9 | 0.26 | 0.9 | 38 | 0.04 |
| S8 | $Tb_{65}Cu_{35}$ | 4 | 24.9 | Yes | 0.04 | 31 | 0.48 | 0.33 | 37 | 0.20 |

volume of the particles. The integrated intensity per cubic ångström of this two-phase system is given by

$$\bar{I}(E) = 2\pi^2\varphi(1-\varphi)[\rho_m(E) - \rho_p(E)][\rho_m(E) - \rho_p(E)]^*. \tag{4}$$

$\varphi$ represents the volume fraction occupied by the particles ($\varphi = N_p V_p / V$).

From equation (3) the relative variations in the intensity obtained near an edge must allow us to identify the nature of the particles by comparison with the theoretical values calculated for the possible kinds of particle. After having identified the particles, the values of the integrated intensities can then be used for estimating their volume fractions from equation (4).

Note that from the values of $\Delta I/I$ we cannot distinguish between RE particles, Cu particles or particles of composition $RE_y Cu_{1-y}$. In fact, on the assumption that the RE concentrations in the amorphous matrix and in the particles are equal to $x$ and $y$ and that the partial volumes $v_{RE}$ and $v_{Cu}$ of the two constituents are identical in the two phases, the SAXS intensity can be rewritten from the work of Maret *et al* (1989) as

$$I(q,E) = (N_p V_p^2/V)(x v_{RE}/v_{am} - y v_{RE}/v_p)^2[f_{RE}(E)/v_{RE} - f_{Cu}(E)/v_{Cu}] \times [f_{RE}(E)/v_{RE} - f_{Cu}(E)/v_{Cu}]^*. \tag{5}$$

Therefore, the $E$-independent term which contains the concentrations $x$ and $y$ does not appear in $\Delta I/I$. In table 2 we give for each edge the values of $\Delta I/I$ corresponding to different kinds of particle distributed in the amorphous matrix, as detected by microprobe analysis. The molecular volumes of the dihydrides and trihydrides are those of the crystalline hydrides (Libowitz and Maeland 1979).

### *4.2. Nature of particles*

The comparison between the experimental and calculated $\Delta I/I$-values given in table 2 indicates that the scattering ring cannot be attributed to a segregation of RE or Cu atoms, since they are associated with values of $\Delta I/I$ near the L edge much larger than the experimental values. Oxide particles or contaminant elements, such as Si and Ar, can also be excluded, leading to values near the K edge either too negative or not sufficiently negative. The $\Delta I/I$-values calculated for rare-earth dihydride and trihydride particles show that for any alloy composition, when the hydrogen-to-metal atom ratio is increased from 2 to 3, $\Delta I/I$ near the L edge decreases while $\Delta I/I$ near the Cu edge increases. The values given for hydrogen bubbles or voids would be the limits for very high ratios. For samples S1, S4, S5, S7 and S8, the experimental values corresponding to both edges are roughly between those of the two stoichiometric hydrides, while the values measured for samples S2, S3 and S6 are between those corresponding to $REH_3$ and hydrogen or voids.

As quoted in table 2, the molecular volume of the stoichiometric hydrides increases with increasing hydrogen-to-RE ratio. Let us assume the existence of the hydride $REH_n$; its electronic density is given by

$$\rho_p(E) = [f_{RE}(E) + n f_H]/v_{hyd}$$

and $\rho_p(E)$ varies mainly with the volume $v_{hyd}$ (since $f_H \ll F_{RE}(E)$). From equation (3), the $\Delta I/I$ variations are then mainly dependent on $v_{hyd}$. The variations in

**Table 2.** Experimental values of the relative variations $\Delta I/I$ in the scattering ring intensities measured near the $L_{III}$ and K edges and calculated values of $\Delta I/I$ for different kinds of particle dispersed in the four amorphous alloys studied (the molecular volumes of these particles are indicated in parentheses).

| Alloy composition | Edge | Experimental $\Delta I/I$ (%) | | | Calculated $\Delta I/I$ (%) | | | | | |
|---|---|---|---|---|---|---|---|---|---|---|
| | | | | | $GdH_2$(36.7 Å$^3$) | $GdH_3$(40.6 Å$^3$) | H or pore | Cu(11.8 Å$^3$) or Gd(33.1 Å$^3$) | $Gd_2O_3$(79 Å$^3$) | Ar (28.5 Å$^3$)[a] or Si (20 Å$^3$) |
| $Gd_{29}Cu_{71}$ | | S1 | S2 | | | | | | | |
| | $L_{III}$ | +26 | +7 | | +39 | +21 | −13 | +74 | +48 | −19 |
| | K | Not measured | −44 | | −66 | −54 | −12.5 | −64 | −79 | −18 |
| $Gd_{70}Cu_{30}$ | | S3 | S4 | | | | | | | |
| | $L_{III}$ | −22 | −4 | | +5 | −10 | −22 | +74 | −32 | −34 |
| | K | −11 | −22 | | −42 | −24 | −2 | −64 | −86 | −3 |

| Alloy composition | Edge | Experimental $\Delta I/I$ (%) | | | Calculated $\Delta I/I$ (%) | | | | | |
|---|---|---|---|---|---|---|---|---|---|---|
| | | | | | $TbH_2$(35.5 Å$^3$) | $TbH_3$(39.5 Å$^3$) | H or pore | Cu(11.8 Å$^3$) or Tb (31.9 Å$^3$) | $Tb_2O_3$(77.4 Å$^3$) | Ar (28.5 Å$^3$) or Si (20 Å$^3$) |
| $Tb_{25}Cu_{75}$ | | S5 | S6 | S7 | | | | | | |
| | $L_{III}$ | +38 | +6 | +34 | +47 | +25 | −12 | +91 | +53 | −18 |
| | K | Not measured | −42 | −60 | −68 | −59 | −12 | −55 | −76 | −17 |
| $Tb_{65}Cu_{35}$ | | S8 | | | | | | | | |
| | $L_{III}$ | +13 | | | +11 | −6 | −21 | +91 | −14 | −31 |
| | K | −37 | | | −50 | −28 | +1 | −55 | −91 | +2 |

[a] For liquid argon at 87 K.

$\Delta I/I$ with $v_{hyd}$ illustrated in figures 5 and 6 for alloys of compositions $Gd_{70}Cu_{30}$ and $Tb_{25}Cu_{75}$ (bold full and broken curves) are calculated by increasing regularly $n$ from 0 to 4 when $v_{hyd}$ increases from 33 to 48 Å$^3$ (this increase is deduced from the molecular volumes of $REH_2$ and $REH_3$). The experimental points are given on these curves; in figure 5, for sample S4 the values of $\Delta I/I$ measured near the L and K edges correspond to the values of $v_{hyd}$ equal to 38 Å$^3$ and 41 Å$^3$, respectively, and for sample S3 a value of about 48 Å$^3$ can be measured for the K edge and an even larger value for the L edge. In figure 6, for samples S6 and S7 of $Tb_{25}Cu_{75}$, each pair of values converges towards similar values of $v_{hyd}$ close to 48 Å$^3$ and 38 Å$^3$, respectively. From the average values of $v_{hyd}$ and the corresponding hydrogen-to-RE ratios, the scattering contrast $\rho_m - \rho_p$ can be calculated and using equation (4) the volume fraction of hydride particles is deduced from the average integrated intensities (given in table 1).

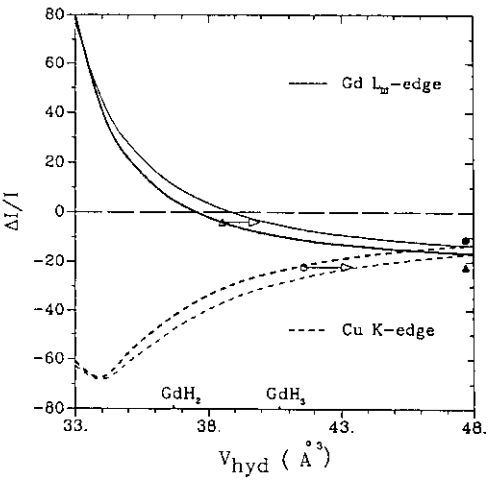


**Figure 5.** Relative variations in the scattering ring intensity when near the $L_{III}$ edge (——, ——) and the K edge (– – –, – – –) as a function of the molecular volume of hydride particle for alloy compositions $Gd_{70}Cu_{30}$ (——, – – –) and $Gd_{64}Cu_{36}$ (——, – – –). The latter composition is that of the remaining amorphous matrix containing a hydride volume fraction of 0.18. The values of $\Delta I/I$ measured near the $L_{III}$ and K edges are indicated, respectively, by triangles and circles for sample S3 (▲, ●) and sample S4 (△, ○).

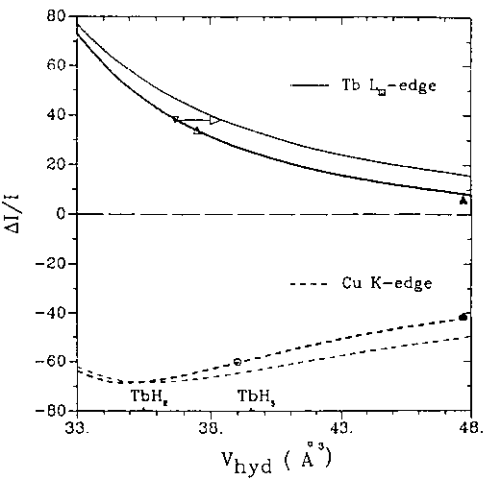


**Figure 6.** Relative variations in the scattering ring intensity when near the $L_{III}$ edge (——, ——) and the K edge (– – –, – – –) as a function of the molecular volume of hydride particle for alloy compositions $Tb_{25}Cu_{75}$ (——, – – –) and $Tb_{14}Cu_{86}$ (——, – – –). The latter composition is that of the remaining amorphous matrix containing a hydride volume fraction of 0.13. The values of $\Delta I/I$ measured near the $L_{III}$ and K edges are indicated, respectively, by triangles and circles for sample S5 (▽), sample S6 (▲, ●) and sample S7 (△, ○).

For large values of $\varphi$ (i.e. $\varphi > 0.1$ for a RE-poor alloy and $\varphi > 0.2$ for a RE-rich alloy) the composition of the remaining amorphous matrix is recalculated taking into consideration the number of RE atoms included in the hydride particles. Therefore the contrast is changed as well as $\Delta I/I = f(v_{hyd})$. As illustrated in figures 5 and 6 (thin full and broken curves), a significant decrease in the RE concentration in the remaining amorphous matrix modifies the curves of $\Delta I/I$ such that the measured $\Delta I/I$ correspond to larger molecular volumes of hydride (as indicated by the arrows for samples S4 and S5). It is worth noting that a significant decrease in the RE

concentration leads the curves of $\Delta I/I = f(v_{hyd})$ corresponding to the two edges to become farther apart, while at a fixed concentration a decrease in the atomic volume of the amorphous alloy due to chemical order effects would bring the two curves closer together (not shown) and the experimental values of $\Delta I/I$ would then correspond to smaller molecular volumes of hydride. In table 1 we report for all the samples the values of the molecular volumes and the volume fractions of the hydride particles ($v_{hyd}$ and $\varphi$ are the average values deduced from the measurements near the two edges and corrected for the decrease in the RE concentration in the remaining amorphous matrix).

### *4.3. Scaling functions*

A way to compare the different patterns is to calculate the scaling function $F(q/q_1, E)$ defined as

$$F(q/q_1, E) = q_1^3 I(q, E)/\tilde{I}(E).$$

$q_1$ is the first moment of $I(q)$. This function was defined for the late stages of phase-separating systems (Lebowitz *et al* 1982). In these stages the precipitate volume fraction is almost constant and thus there is for the system only one pertinent scaling length proportional to $1/q_1$: the width $\Delta X$ of the scaled interference ring. From the work of Bley *et al* (1991), $\Delta X$ decreases slightly when increasing the volume fraction from about 0.8 for $f = 0.04$, to 0.6 for $f > 0.15$.

Figures 7 and 8 show the functions $F(q/q_1, E)$ calculated for the samples S3 and S6 and corresponding to the different energies chosen below the L edge; for both samples all the curves are well superimposed. Note that the functions corresponding to the energies below the K edge (not presented in figures 7 and 8) are also superimposed on these curves.

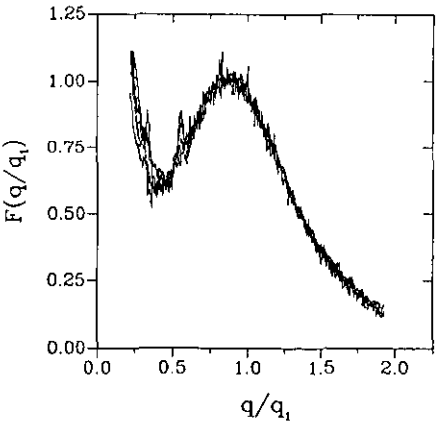


**Figure 7.** Scaling functions of the scattering intensities corresponding to the five energies chosen below the Gd $L_{III}$ edge for the amorphous alloy $Gd_{70}Cu_{30}$ (sample S3). $q_1$ is the first moment of $I(q)$.

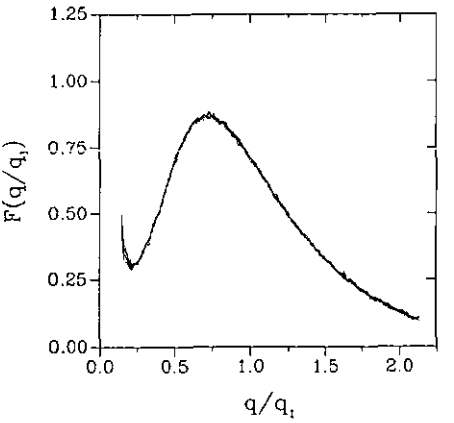


**Figure 8.** Scaling functions of the scattering intensities corresponding to the five energies chosen below the Tb $L_{III}$ edge for the amorphous alloy $Tb_{25}Cu_{75}$ (sample S6).

The shape of the scaling functions calculated for the other samples is similar to those shown in figures 7 and 8 and indicates that the interference effects between particles are independent of the hydride composition. Here, most of the samples exhibit a width equal to unity, except sample S8 ($\Delta X = 0.93$). The fact that $\Delta X$ is too large and does not vary with $\varphi$ could be attributed to a large distribution of particle sizes in a given sample. Such a distribution would also explain why the $Iq^4$ versus $q$ plots of these amorphous alloys do not present a well defined maximum as observed for narrow-sized dispersions such as in Al–Zn alloys (Guilarducci *et al* 1987).

### *4.4. Concluding remarks*

Except for samples S3 and S6, the compositions of the hydride particles deduced from the values of $v_{hyd}$ given in table 1 are close to that of the trihydride. The molecular volumes for samples S3 and S6 are much larger than those of the trihydrides and for sample S3 the value of $\Delta I/I$ measured near the L edge is equal to the value calculated for hydrogen bubbles. These large molecular volumes of hydride are, however, not associated with the largest volume fractions. Since the compositions of the crystalline RE hydrides do not extend beyond a RE-to-hydrogen ratio of 3, we suggest that in samples S3 and S6 the trihydride particles contain some porosity which can explain molecular volumes as large as 48 Å$^3$. For small particles, such as those in sample S3 ($R_g \simeq 5$ Å), the definition of a phase becomes difficult and there is no clear structural difference between bubbles of hydrogen atoms and particles of porous RE hydrides.

## Acknowledgment

We would like to thank N Valignat for the microprobe measurements.

## References

Bley F, Guyot P, Livet F and Simon J P 1991 *Phase Transitions* **31** 201
Boucher B and Chieux P 1991 *J. Phys.: Condens. Matter* **3** 2207
Boucher B, Chieux P, Convert P, Tourbot R and Tournarie M 1986 *J. Phys. F: Met. Phys.* **16** 1821
Boucher B, Chieux P, Convert P and Tournarie M 1983 *J. Phys. F: Met. Phys.* **13** 1339
Boucher B, Elgadi M, Sanquer M, Tourbot R, Bigot J, Chieux P, Convert P and Bellissent-Funel M C 1988 *Z. Phys. Chem., NF* **157** 23
Chieux P, de Kouchkovsky R and Boucher B 1984 *J. Phys. F: Met. Phys.* **14** 2239
Dubuisson J M, Dauvergne J M, Depautex C, Vachette P and Williams C E 1986 *Nucl. Instrum. Methods* A **246** 636
Goudeau P, Naudon A, Chamberod A, Rodmacq B and Williams C E 1987 *Europhys. Lett.* **3** 269
Guilarducci de Salva A, Simon J P, Livet F and Guyot P 1987 *Scr. Metall.* **21** 1061
Lebowitz J L, Marro J and Kalos M M 1982 *Acta Metall.* **30** 297
Libowitz G G and Maeland A J 1979 *Handbook on the Physics and Chemistry of Rare Earths* ed K A Gschneider and L Eyring (Amsterdam: North-Holland) p 299
Lyon O and Simon J P 1987 *Phys. Rev.* B **35** 5164
Maret M, Simon J P and Lyon O 1989 *J. Phys.: Condens. Matter* **1** 10249
Sazaki S 1984 *National Laboratory for High-Energy Physics, Tsukuba, Japan, Report* KEK 83.22